

Supporting Information

Fluorinated Fullerene Interlayers for Tin Halide Perovskite Solar Cells with Enhanced Operational Air Stability and Minimized Voltage Losses

Sergio Galve-Lahoz,^{1,2} Jesús Sánchez-Díaz,¹ Jorge Marco-Guimbao,² Nihal Guenani,¹ Jorge Simancas,¹ Jhonatan Rodriguez-Pereira,^{3,4} Jesús Lucia-Tamudo,⁵ Sergio Díaz-Tendero,^{6,7,8} Jorge Pascual,² Beatriz Julián-López,¹ Juan P. Martínez-Pastor,⁹ Eva M Barea,¹ Iván Mora-Seró^{1} and Juan Luis Delgado^{2,10*}*

¹Institute of Advanced Materials (INAM), University Jaume I, Av. Vicent Sos Baynat, s/n, 12071, Castellón de la Plana, Spain

²Polymat, University of the Basque Country UPV/EHU, 20018 Donostia-San Sebastian, Spain

³Center of Materials and Nanotechnologies, Faculty of Chemical Technology, University of Pardubice, nám. Cs. legií 565, Pardubice, 53002, Czech Republic

⁴Central European Institute of Technology, Brno University of Technology, Purkynova 123, Brno, 612 00, Czech Republic

⁵Faculty of Chemistry and Pharmacy, Institute of Physical and Theoretical Chemistry, University of Regensburg, 93040 Regensburg, Germany.

⁶Department of Chemistry, Universidad Autónoma de Madrid, 28049, Madrid, Spain

⁷Institute for Advanced Research in Chemistry (IAdChem), Universidad Autónoma de Madrid, 28049 Madrid, Spain

⁸Condensed Matter Physics Center (IFIMAC), Universidad Autónoma de Madrid, 28049 Madrid, Spain

⁹Instituto de Ciencia de los Materiales (ICMUV), Universitat de Valencia, 46980 Paterna, Spain

¹⁰Ikerbasque, Basque Foundation for Science, Bilbao 48013, Spain

*Corresponding authors: sero@uji.es, juanluis.delgado@polymat.eu

Materials

Chemicals and solvents for the synthesis were purchased from Sigma-Aldrich and Thermo Scientific, and used as received without additional purification. Anhydrous solvents were dried using a Pure Solve solvent purification system. Column chromatography was performed using silica gel (40 to 60 μm) from Sigma Aldrich as the stationary phase, and thin layer chromatography (TLC) was conducted on pre-coated silica gel. The materials used in the photovoltaic study were obtained from commercial suppliers in high purity and employed without further purification: Formamidinium iodide (FAI, 99.99%), di-propylammonium iodide (DipI), and di-propylammonium chloride (DipCl) were purchased from Greatcell Solar Materials. C_{60} (99.95%) was obtained from Nano-C. Phenethylammonium iodide (98%), tin (II) iodide (SnI_2 , 99.99%), tin (II) fluoride (SnF_2 , 99%), bathocuproine (BCP, 99.99%), *N,N*-dimethylformamide (DMF, 99.8%), dimethylsulfoxide (DMSO, 99.8%) were purchased from Sigma-Aldrich. PEDOT:PSS AI 4083 aqueous solution was purchased from Heraeus.

Device fabrication

2.5 x 2.5 cm pre-patterned ITO substrates were washed in subsequent ultrasonic baths for 15 minutes each. First, the substrates were washed with water and soap and rinsed with milli-Q water. Then, the substrates were washed with acetone and isopropanol and finally dried with N_2 flow. A 15 minutes UV-Ozone treatment was performed strictly before the HTM deposition.

For the deposition of the HTM, a PEDOT:PSS solution was filtered with 0.45 μm PVDF filter and spin-coated on top of the ITO substrates at 3500 $\text{rpm}\cdot\text{s}^{-1}$ for 40 s and then annealed at 125°C for 30 minutes. Thereafter, the substrates were immediately introduced into a N_2 -filled glovebox for the perovskite layer deposition (FA, formamidinium). The $\text{FA}_{0.9}\text{Dip}_{0.08}\text{PEA}_{0.02}\text{SnI}_{2.95}\text{Cl}_{0.05}$ perovskite precursor are composed of 0.9 M SnI_2 , 0.81 M FAI, 0.045 M DipCl, 0.027 M DipI, 0.018 M PEAI, and 0.1 M SnF_2 solved in DMSO:DMF (9:1 V/V) mixed solvent and stirred overnight. The perovskite solution was spin-coated on top of PEDOT:PSS at 4000 rpm for 50s. After 27 seconds of spinning, 400 μL of chlorobenzene were dropped on the substrate to induce perovskite crystallization, followed by a two-step annealing at 70°C for 1 minute and 100°C for 20 minutes. For the devices incorporating the interlayers, a 0.5 mM solution of **JM10** or **JM12** in chlorobenzene was dynamically spin-coated at 4000 rpm for 30 seconds, and the resulting films were annealed at 100°C for 2 minutes. As an electron transport layer, 30 nm of C_{60} were thermally evaporated on top of the perovskite layer, followed by 6 nm of BCP as a buffer layer and 110 nm of Ag as metal contact. Finally, a three-day light soaking treatment was performed as part of device fabrication.¹

Molecular characterization

Nuclear magnetic resonance (NMR) spectroscopy

All the NMR spectra were recorded on a Bruker Advance 300 (400 MHz for ^1H NMR; 100 MHz for ^{13}C NMR and 376 MHz for ^{19}F NMR) spectrometer at 298 K and referenced to deuterated solvent (e.g., CHCl_3 -d corrected to 7.26 and 77.16 ppm for ^1H and ^{13}C NMR spectra, respectively). Coupling constants (J) are given in Hz and chemical shifts (δ) are reported in ppm. Multiplicities are denoted as follows: s (singlet), d (doublet), t (triplet), q (quartet), dd (doublet of doublets), m (multiplet), br s (broad singlet), br m (broad multiplet).

Mass spectrometry

High-Resolution Matrix-Assisted Laser Desorption Ionization, coupled to a Time-Of-Flight (TOF) analyzer experiments (MALDI-TOF) were carried out on a Bruker Ultraflex III spectrometer. All data were recorded at a maximum accelerating potential of 20 kV in the linear negative ion mode. DCTB was used as a matrix and AgTFA was added as the cationic ionization agent.

Cyclic voltammetry

A three-electrode cell with a platinum working electrode, a platinum counter electrode, and a AgNO₃ reference electrode was employed. The electrolyte consisted of a solution of tetrabutylammonium hexafluorophosphate (NBu₄PF₆) in a solvent mixture of acetonitrile: *o*-dichlorobenzene (1:4) to ensure the proper solubility of the compounds, and the well-known ferrocenium/ferrocene (Fc⁺/Fc) redox couple was used as internal standard. Under these conditions, previous reports determined the formal potential of Fc⁺/Fc to be 0.41 V versus saturated calomel electrode (SCE), corresponding to -5.1 eV on the Fermi scale.² Accordingly, the LUMO energy level (E_{LUMO}) can be estimated using the following equation:³

$$E_{LUMO} = -(E_{[onset,red\ vs.\ Fc^+/Fc]} + 5.1) (eV)$$

Structural characterization

X-ray diffraction (XRD)

XRD patterns of the films were measured using a powder X-ray diffractometer (D8 Advance, Bruker-AXS) in a Bragg-Bretano geometry, using Cu K α X-ray radiation ($\lambda_1 = 1.5406 \text{ \AA}$, $\lambda_2 = 1.5444 \text{ \AA}$, $I_2/I_1 = 0.5$), with a tube voltage and intensity of 40 kV and 40 mA, respectively. The goniometer arm length was 217.5 mm, using a divergence slit fixed at 0.6°. The detector was a BRUKER-

binary V3, using a scan range from 5.0° to 70.0° (2θ °), with a scan step size of 0.02 (2θ °) and a counting time of 75 s/step. Measurements were registered at room temperature (298 K).

Scanning Electron Microscope (SEM)

The topographical and cross-sectional images were taken using a field emission scanning electron microscope (FEG-SEM) JEOL 3100F operated at 15 kV. The SEM images were recorded from films deposited on top of ITO covered substrates.

X-ray Photoelectron Spectroscopy (XPS)

The surface chemical composition and electronic state of perovskites films with and without **JM10** and **JM12** were determined by XPS (ESCA-2SR, Scienta-Omicron). Spectra were recorded using monochromatic Al $K\alpha$ = 1486.6 eV operated at 100 W. The binding energy scale was referenced to adventitious carbon (284.8 eV). CasaXPS processing software (Casa software Ltd) was used to analyze the data and the quantitative analysis was made using sensitivity factors provided by the manufacturer.

Water contact angle

The water contact angle was measured using a Kruss DSA25E Drop Shape Analyzer by dropping a droplet of deionized water onto the different substrates. A 30-seconds video was recorded registering the behavior of the drop until its stabilization and the contact angle of the stable drop was measured using the DSA25E built-in software.

Optoelectronic characterization

UV-Vis Absorption Spectra

The absorption spectra were recorded using a Varian Cary 300 UV/Vis absorption spectrophotometer. UV-Vis spectra were recorded from films deposited on glass substrates.

Steady-state Photoluminescence (PL) and Time-Resolved PL (TRPL)

The PL and TRPL characterization of the different fabricated samples was carried out at room temperature and vacuum conditions, in order to avoid any oxidation effect during the measurements and hence having identical conditions for all samples (that were conveniently packed inside the glove box where they were prepared). The characterization was performed in a 90° excitation-detection backscattering configuration using a high-resolution Edinburgh FLS1000 system using an excitation wavelength of 465 nm produced by a Xe lamp for PL or a supercontinuum pulsed laser (FYLA SCT1000) for TRPL, both filtered by the excitation double monochromator of the system. The detection for both PL and TRPL was performed with a cooled PMT-980 photomultiplier or a near infrared one (Hamamatsu H10330-75). The overall time resolution was in the range of 0.3-0.4 ns, because any deconvolution was applied for extracting the characteristic decay times.

Solar Cell Performance Measurement

The current density -voltage (J - V) curves were measured using an Abet technologies (Sun, 2,000) solar simulator. The light intensity was adjusted to 1 sun ($100 \text{ mW}\cdot\text{cm}^{-2}$) using a calibrated Si solar cell and a photodiode. The devices were measured in ambient conditions and without any encapsulation. The active area of the cells is defined with a 0.26 cm^2 mask.

Maximum Power Point Measurement

Measurements were performed under 1 sun ($100 \text{ mW}\cdot\text{cm}^{-2}$) continuous illumination, using an Abet technologies (Sun, 2,000) solar simulator calibrated with a Si solar cell and a photodiode. The measurements were performed with an AUTOLAB (PGSTAT30) potentiostat. Fixed voltages corresponding to the initially measured V_{MPP} were applied, which were obtained from the J - V curves, and the electrical current I_{MPP} was monitored over time. Note that devices were characterized without receiving the previously commented light-soaking treatment.

Computational details and results

All electronic structure calculations related to the adsorption of fullerene derivatives on the FASnI_3 perovskite were performed using VASP.⁴⁻⁹ For calculations involving fullerene properties, the ORCA software was used.¹⁰

Dipole Moment

The geometry of the fullerene derivatives was optimized at the OPTPBE/def2-TZVPP level of theory.¹¹⁻¹⁷ The energy and properties of these compounds were determined using the same methodology and including the D3 correction by Perdew *et al.*¹⁸ over the geometry previously optimized. Although the dipole moment of a species depends on the reference origin, all coordinates were standardized to the geometric center of the fullerene core, excluding the substituents. This approach allows to have a direct comparison of the dipole moments of all compounds. The molecular electrostatic potentials (MEPs)¹⁹ for each species were carried out with the Multiwfn code²⁰ using the DFT wavefunctions.

Perovskite Modelling

Calculations were performed at the OPTPBE level of theory,¹¹⁻¹⁴ using a plane-wave basis set with a cutoff energy of 420 eV at the Γ point. Convergence criteria were set to 10^{-5} eV for the electronic energy in the SCF cycles, and $5 \cdot 10^{-3}$ eV/Å for forces. First, the geometry of the formamidinium ion was optimized, and the obtained equilibrium structure was then incorporated into an FASnI_3 unit cell. We then optimized the unit cell of the perovskite in two ways: by allowing only the cell lengths to vary, or by allowing both the lengths and angles to adjust. The lattice parameters obtained in the first optimization approach were $a = 5.824$ Å, $b = 5.824$ Å, and $c = 6.656$ Å, keeping a tetragonal cell with $\alpha = \beta = \gamma = 90$. When both cell dimensions and angles were optimized, the computed parameters were $a = 6.196$ Å, $b = 6.164$ Å, $c = 6.352$ Å, $\alpha = 89.45$, $\beta = 84.35$, and $\gamma = 88.26$. These results align well with those previously reported in the literature.^{21, 22} However, calculations for the monoclinic cell were computationally very demanding. Since we are interested in the description of the interaction of fullerene derivatives

with the perovskite surfaces, we used the tetragonal model, which allows us to save computing time without losing accuracy in the simulations.

Setup of the Systems

As shown in Figure S14, we have considered the adsorption of C_{60} , **JM10**, and **JM12** on two different $FASnI_3$ surfaces: one in which the outer layer directly interacts with the fullerene, consisted of a truncated triiodostannate octahedra, and another in which the octahedra remained intact, referred to as SnI_2 -terminated and FAl -terminated, respectively. Both designs were applied to investigate the adsorption of C_{60} fullerene, and the considered derivatives. For the $FASnI_3$ /**JM10** and $FASnI_3$ /**JM12** cases, fullerene orientation is expected to influence the interaction with the perovskite surface. Therefore, three initial fullerene orientations were modeled for each surface type, see Figure S14: fullerene cage-surface interaction (labeled “up”), both fullerene and fluorinated moiety-surface interaction (labeled “middle”), and fluorinated moiety-surface interaction (labeled “down”). The dimensions of the $FASnI_3/C_{60}$ systems were $11.648 \text{ \AA} \times 11.648 \text{ \AA} \times 50.000 \text{ \AA}$, while for the substituted $FASnI_3/C_{60}$ the unit cell lengths were $17.472 \text{ \AA} \times 17.472 \text{ \AA} \times 55.000 \text{ \AA}$. Note that for the $FASnI_3/C_{60}$ systems the perovskite unit cell was replicated twice on the X and Y axes while for $FASnI_3$ /**JM10**(**JM12**) three unit cells were used to establish the dimensions of X and Y. In all the cases the $FASnI_3$ unit cell was replicated five times along the Z axis. A large vacuum gap was included along the Z axis, perpendicular to the surface, to avoid interaction between two adjacent unit cells of the whole system within that direction.

Geometry and Electronic Structure

To optimize the geometry of each fullerene-perovskite system, a preliminary rigid scan (without geometry optimization) was conducted, varying the distance between the fullerene center of mass and the outermost layer of bulk $FASnI_3$. Once the distance at which the system energy is minimized was identified in the scan, this structure was used as a starting point for partial

optimization of the geometry. Only the atoms in the fullerene derivative and in the two outer layers of the perovskite bulk were allowed to change their positions. In the geometry optimization, we employed the OPTPBE functional with a plane-wave basis set at a 420 eV cutoff. Convergence was considered achieved when the change in electronic energy between two adjacent optimization steps was less than 10^{-4} eV and the largest force was less than 10^{-2} eV/Å. The equilibrium energy of each system, the energy of the isolated fullerene, and that of the isolated surface (both in fixed geometries) were calculated to determine the interaction energy and the changes in the electron density due to fullerene/FASnI₃ interaction. The interaction energy was computed as

$$E_{Ads} = E_{surf+mol} - [E_{surf} + E_{mol}]$$

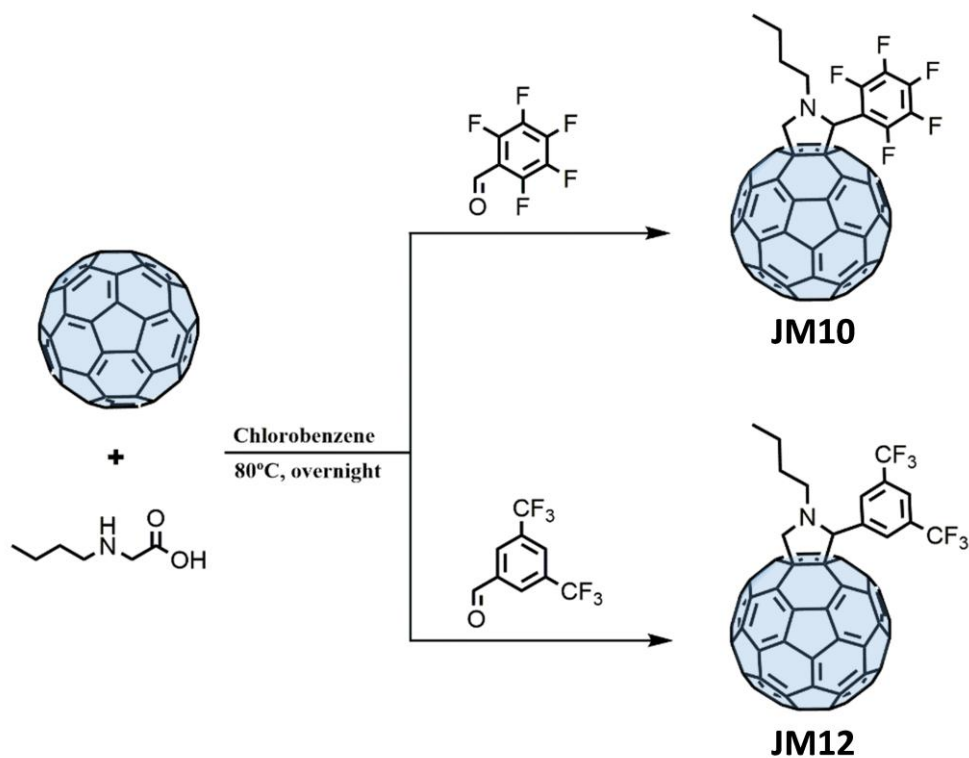
being $E_{surf+mol}$, E_{surf} , and E_{mol} , the electronic energies of the complete system, the surface and the molecule respectively. Similarly, changes in the electronic density upon adsorption were computed as

$$\Delta\rho = \rho_{surf+mol} - [\rho_{surf} + \rho_{mol}]$$

being $\rho_{surf+mol}$, ρ_{surf} , and ρ_{mol} the electronic densities of the complete system, the surface and the molecule, respectively, keeping the optimized geometry upon adsorption.

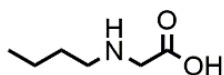
Synthesis of **JM10** and **JM12**

The synthesis of **JM10** and **JM12** are depicted in Scheme S1. All the details and spectroscopy data are described below.



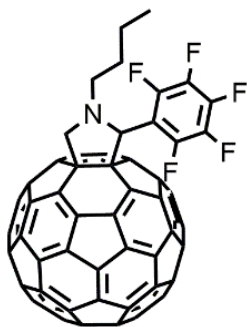
Scheme S1. Synthetic route of **JM10** and **JM12**.

***N*-Butylglycine**



N-Butylglycine was synthesized according to a literature procedure:²³ Butylamine (7.00 g, 96 mmol) was dissolved in a mixture of EtOH (13.5 mL) and water (6.52 mL). After cooling to 0°C, iodoacetic acid (4.00 g, 22 mmol) was added slowly, portionwise. The reaction mixture was stirred for 20 h, allowing it to reach room temperature, and was then poured into 100 mL of acetone. The resulting white precipitate was filtered, washed with acetone, and dried under vacuum (2.04 g, 70%).

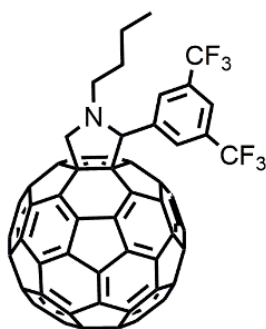
JM10



A solution of C₆₀ (730 mg, 1.00 mmol), pentafluorobenzaldehyde (98 mg, 0.51 mmol), and *N*-butylglycine (262 mg, 2.00 mmol) in chlorobenzene under an Ar atmosphere was refluxed until the reaction was complete. The resulting residue was purified by two successive chromatographic columns: the first one using CS₂ as the eluent, followed by the second one with a 1:1 mixture of CS₂/cyclohexane, yielding the final compound as a brown powder (261 mg, 52%). ¹H NMR (400 MHz, CDCl₃): δ = 5.58 (s, 1H), 5.13 (d, J = 9.3 Hz, 1H), 4.08 (dd, J = 9.4, 3.0 Hz, 1H), 3.17 (dt, J = 11.7, 8.3 Hz, 1H), 2.70 (m, 1H), 2.04 (m, 1H), 1.90 (m, 1H), 1.76 (m, 1H), 1.62 (m, 1H), 1.13 (t, J = 7.3 Hz, 3H). ¹³C NMR (100 MHz, CDCl₃): δ = 192.31, 155.28, 153.08, 151.98, 150.69, 147.14, 146.15, 146.02, 145.94, 145.91, 145.86, 145.81, 145.50, 145.41, 145.30, 145.27,

145.24, 145.19, 145.17, 145.09, 145.04, 144.96, 144.55, 144.33, 144.24, 144.12, 142.95, 142.89, 142.55, 142.46, 142.05, 141.99, 141.91, 141.76, 141.52, 141.49, 141.44, 140.17, 140.10, 140.08, 139.43, 137.89, 136.50, 135.65, 135.33, 129.49, 128.47, 111.49, 74.87, 73.70, 73.66, 68.83, 66.30, 53.44, 30.59, 21.04, 14.47. **¹⁹F NMR** (376 MHz, CDCl₃): δ = -131.05 (dt, J = 22.8, 7.2 Hz, 1F), -138.83 (dt, J = 23.6, 7.1 Hz, 1F), -150.89 (td, J = 21.8, 3.1 Hz, 1F), -158.10 (td, J = 22.4, 7.8 Hz, 1F), -159.27 (td, J = 22.7, 9.0 Hz, 1F). **MALDI-TOF-MS**: m/z 984.07 (100%, [M-H]⁺, calculated for C₇₂H₁₂F₅N: 984.01)

JM12



A solution of C₆₀ (730 mg, 1 mmol), 3,5-Bis(trifluoromethyl)benzaldehyde (121 mg, 0.5 mmol), and *N*-Butylglycine (262 mg, 2.00 mmol) in chlorobenzene under an Ar atmosphere was heated to reflux until the reaction was complete. The resulting mixture was purified using two chromatographic columns: the first one using CS₂ as the eluent, followed by the second with a 1:1 mixture of CS₂/cyclohexane. The final compound, **JM12**, was obtained as a brown powder (289 mg, 56%). **¹H NMR** (400 MHz, CDCl₃): δ = 8.30 (s, 2H), 7.86 (s, 1H), 5.21 (s, 1H), 5.18 (d, J = 9.5 Hz, 1H), 4.20 (d, J = 9.4 Hz, 1H), 3.15 (dt, J = 12.2, 8.2 Hz, 1H), 2.67 (m, 1H), 2.04 (m, 1H), 1.88 (m, 1H), 1.78 (m, 1H), 1.63 (m, 1H), 1.11 (t, J = 7.3 Hz, 3H). **¹³C NMR** (100 MHz, CDCl₃): δ = 192.43, 155.55, 153.28, 152.00, 151.36, 147.27, 147.25, 146.28, 146.17, 146.15, 146.11, 146.09, 145.92, 145.90, 145.68, 145.59, 145.55, 145.37, 145.34, 145.32, 145.28, 145.21, 145.16, 145.13, 144.89, 144.66, 144.47, 144.36, 144.24, 143.13, 143.00, 142.70, 142.60, 142.57, 142.51, 142.21,

142.14, 142.11, 141.99, 141.90, 141.87, 141.74, 141.66, 141.63, 141.58, 140.58, 140.30, 140.26,
140.10, 139.51, 137.06, 136.17, 136.11, 135.52, 131.91, 131.64, 129.42, 129.39, 126.25, 124.08,
122.26, 122.23, 122.20, 121.91, 119.73, 81.45, 75.90, 68.59, 66.69, 52.95, 30.64, 20.86, 14.29.
¹⁹F NMR (376 MHz, CDCl₃): δ = 62.53 (s, 6F). **MALDI-TOF-MS:** m/z 1032.11 (100%, [M+H]⁺,
calculated for C₇₂H₁₂F₅N: 1032.11).

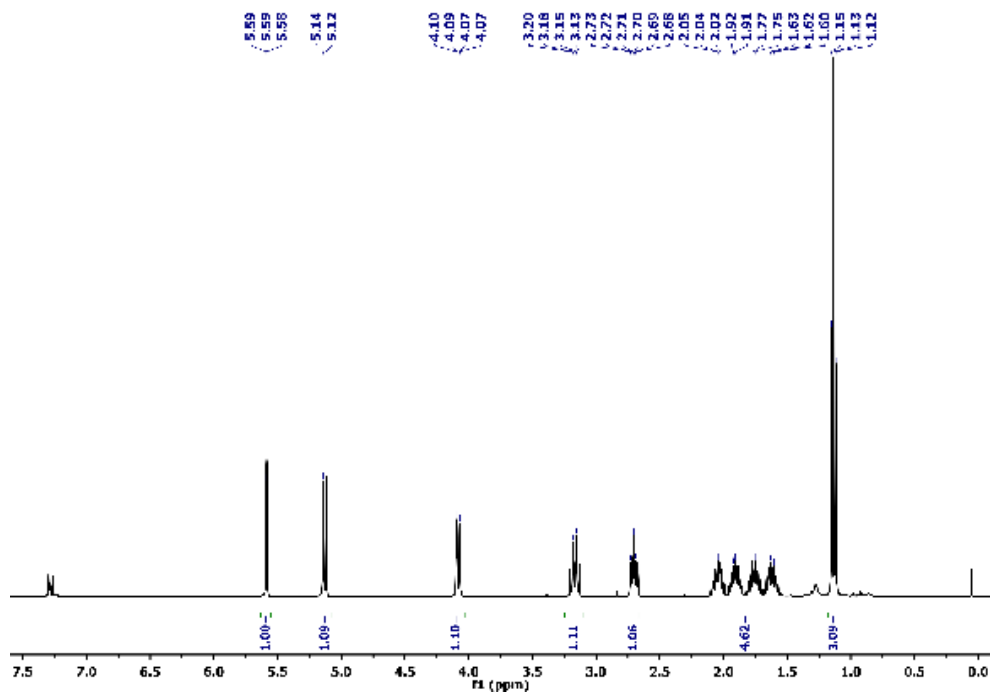


Figure S1. ^1H NMR spectrum (400 MHz, CDCl_3 , 298 K) of JM10.

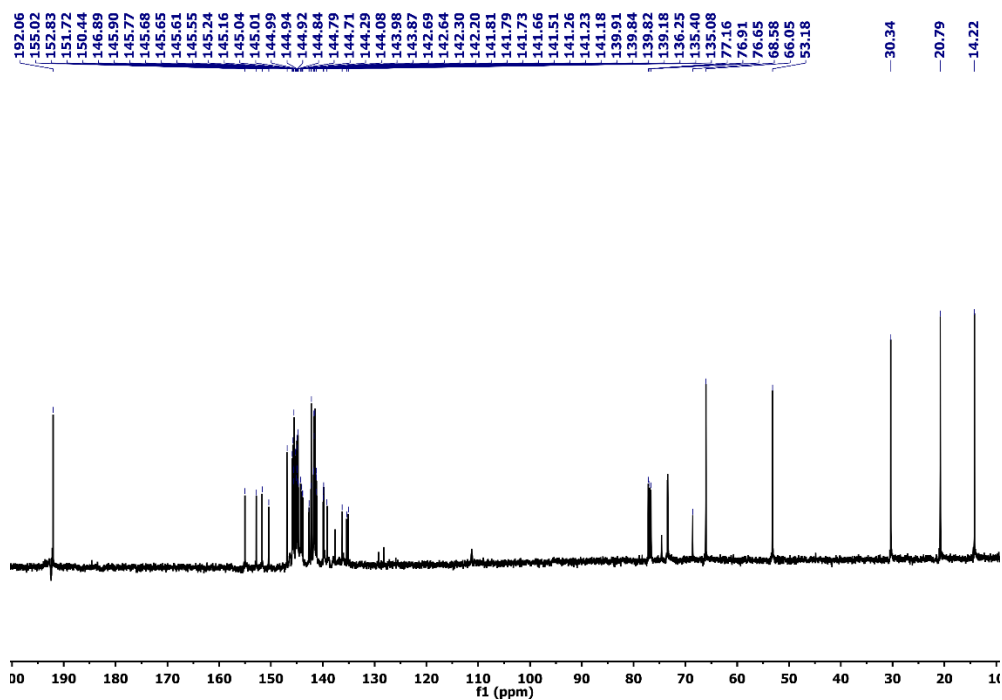


Figure S2. ^{13}C NMR spectrum (100 MHz, CDCl_3 , 298 K) of JM10.

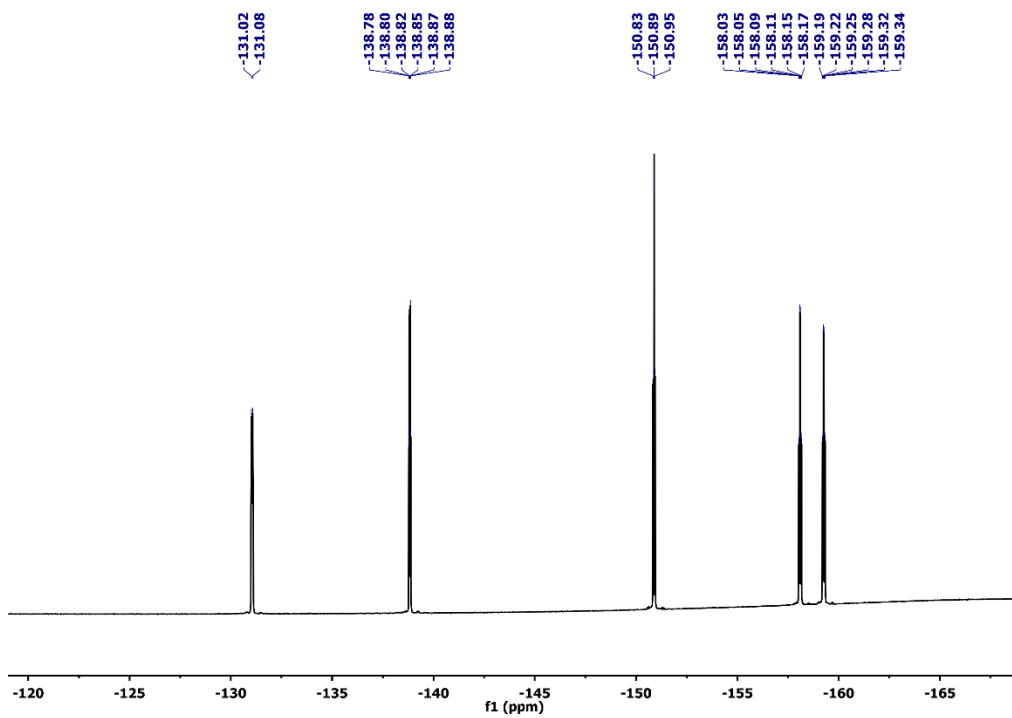


Figure S3. ^{19}F NMR spectrum (376 MHz, CDCl_3 , 298 K) of JM10.

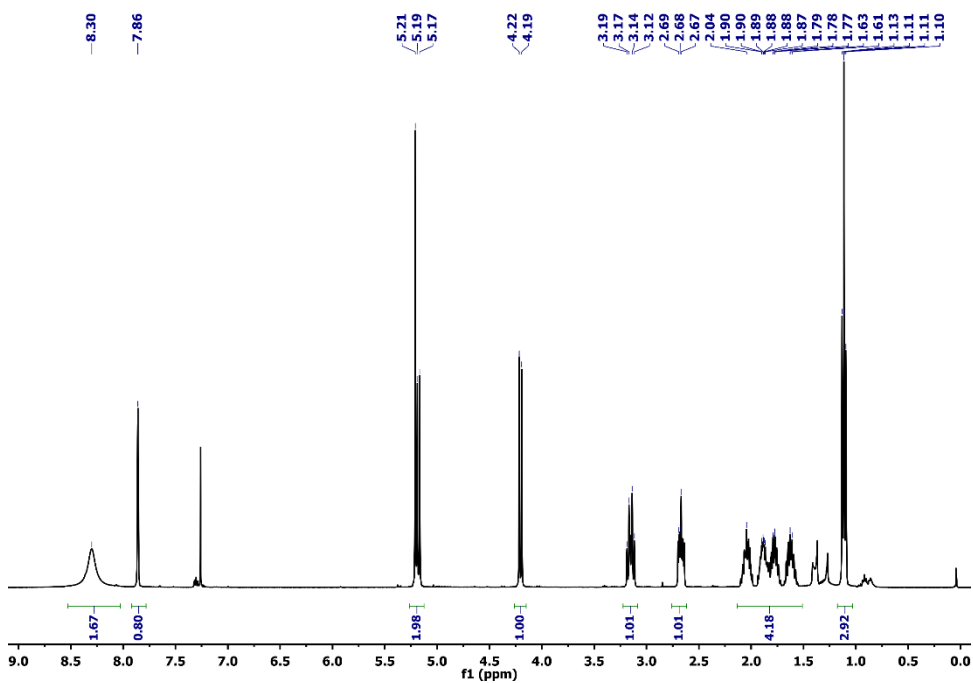


Figure S4. ^1H NMR spectrum (400 MHz, CDCl_3 , 298 K) of JM12.

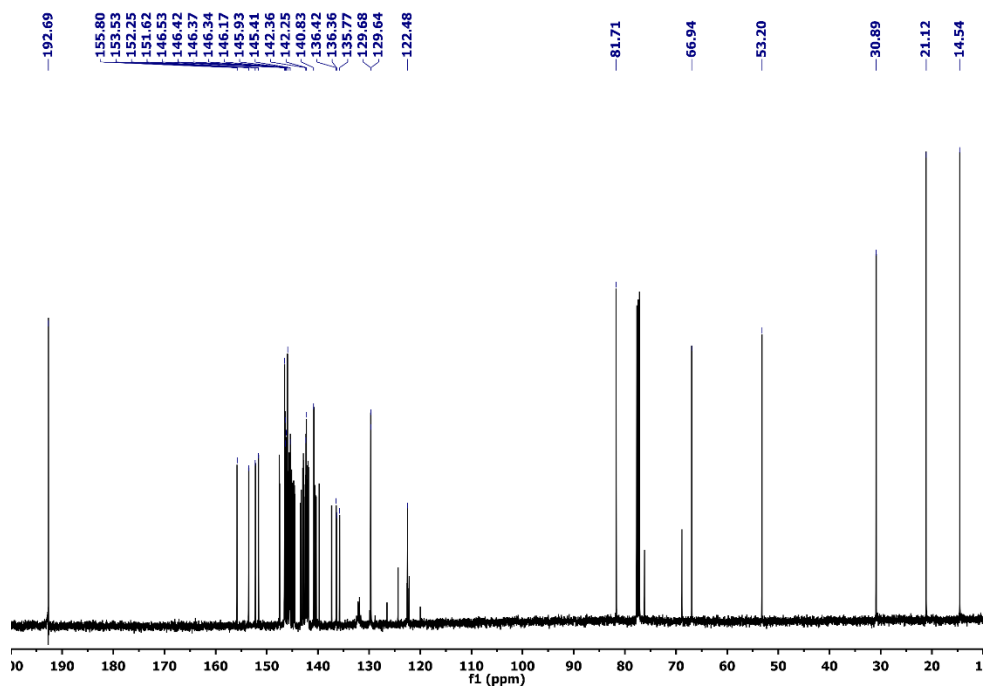


Figure S5. ¹³C NMR spectrum (100 MHz, CDCl₃, 298 K) of JM12.

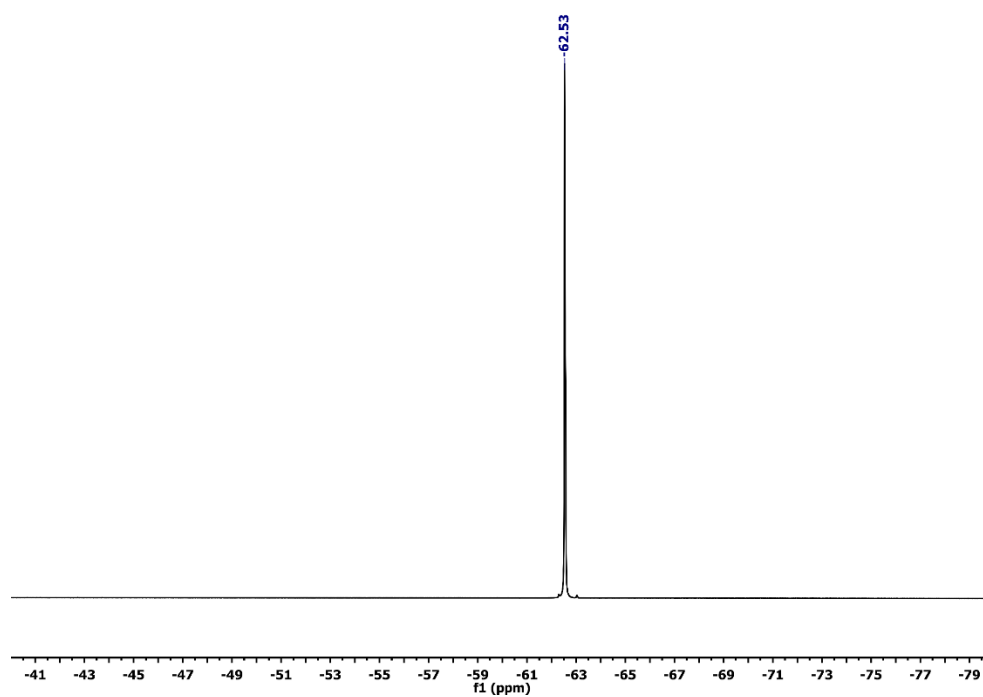


Figure S6. ¹⁹F NMR spectrum (376 MHz, CDCl₃, 298 K) of JM12.

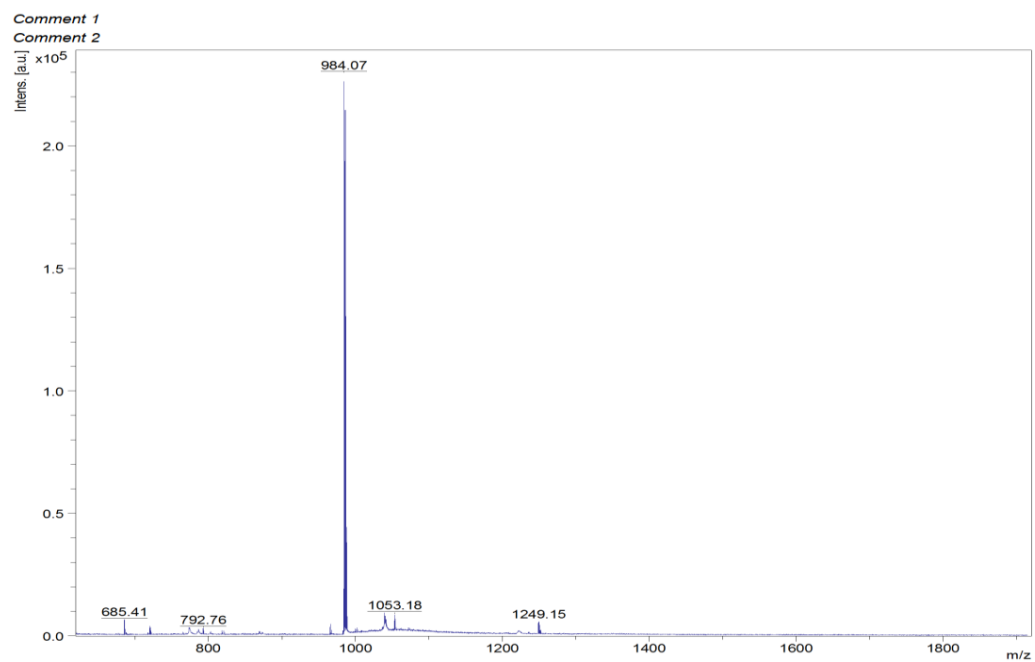


Figure S7. MALDI-TOF mass spectrum of JM10.

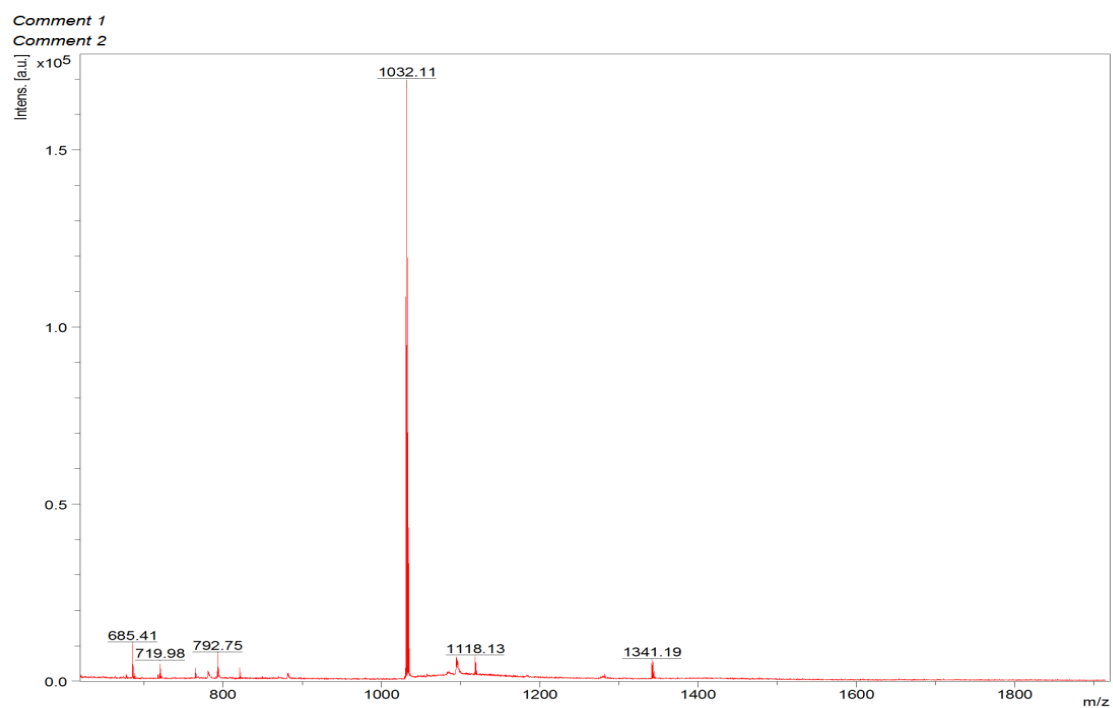


Figure S8. MALDI-TOF mass spectrum of JM12.

Table S1. Optical and energetic parameters of the different fullerene derivatives.

Compound	$\lambda_{\text{abs max}}$ (nm)	E_g (eV)	$E_{\text{red}}^{1/2}$ (V)	ϵ_{LUMO} (eV)	ϵ_{HOMO} (eV)
C₆₀	624	1.98	-1.05	-4.05	-6.03
JM10	701	1.77	-1.12	-3.98	-5.75
JM12	702	1.76	-1.09	-4.01	-5.77

Table S2. Dipole moment of different fullerene derivatives calculated using DFT calculations.

Compound	μ (x, y, z) (a.u.)	μ (a.u.)
C₆₀	(0.000004, -0.000038, -0.000027)	0.000046
JM8	(0.131176, -0.938584, 0.265850)	0.984289
JM9	(0.180287, -0.977389, 0.269470)	1.029761
JM10	(-0.912094, -0.315551, -0.743696)	1.218430
JM12	(-0.995069, -0.124216, -0.861319)	1.321916

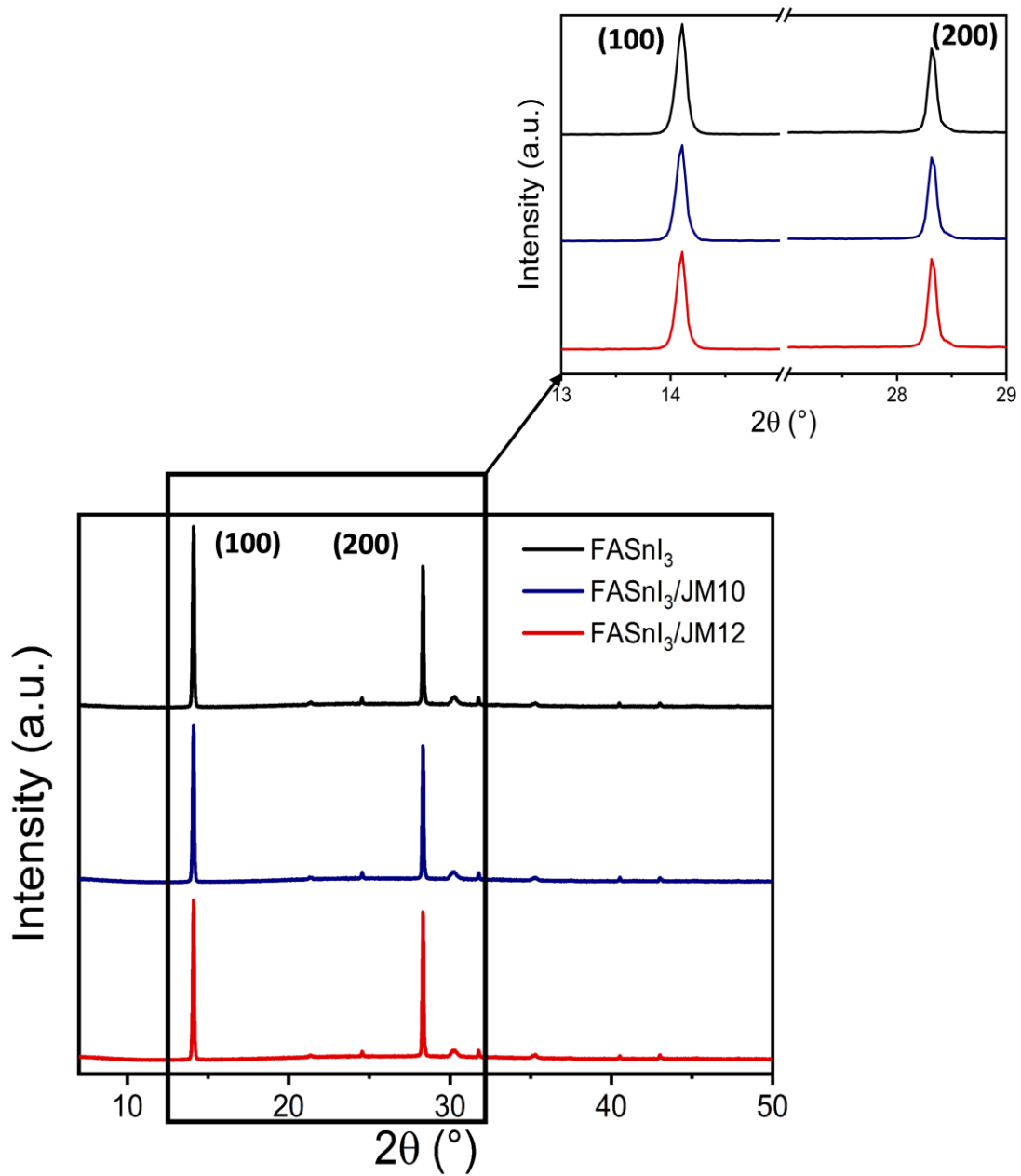


Figure S9. X-ray diffraction patterns for different perovskite films.

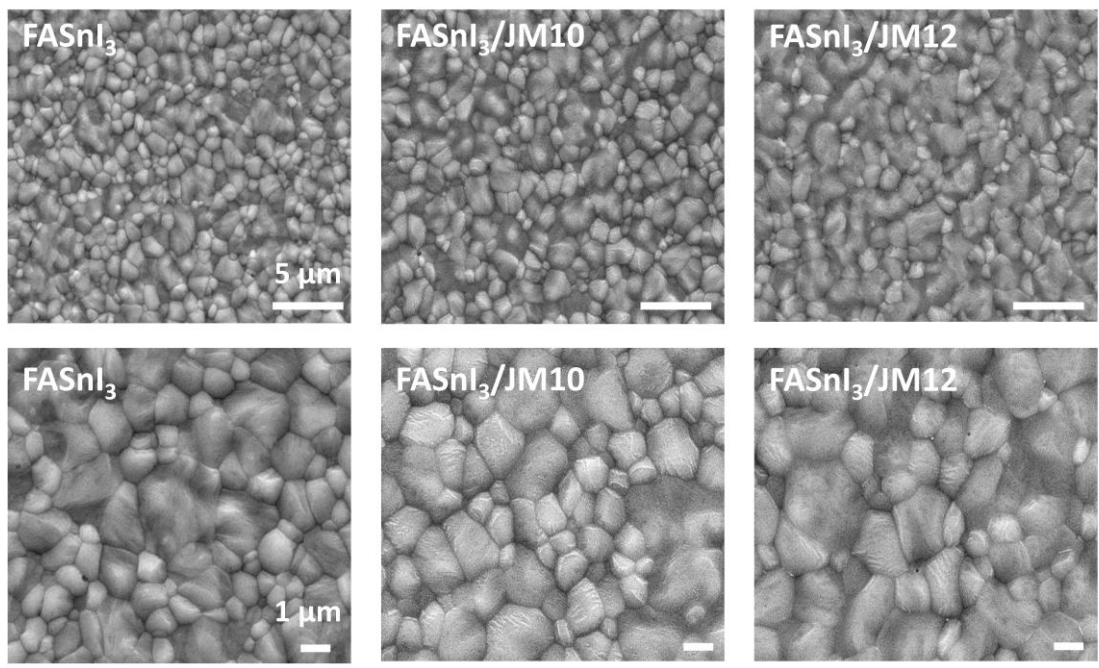


Figure S10. SEM images for different perovskite films at lower (top) and higher (bottom) magnifications.

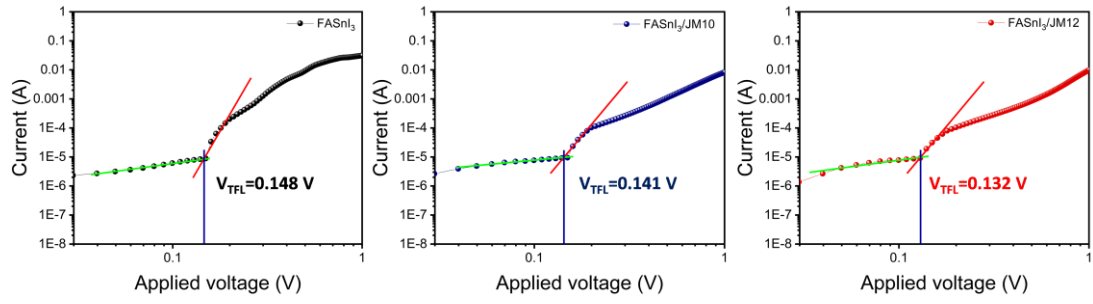


Figure S11. Space charge-limited current (SCLC) measurements of the electron-only devices for (a) control, (b) **JM10**, and (c) **JM12** devices.

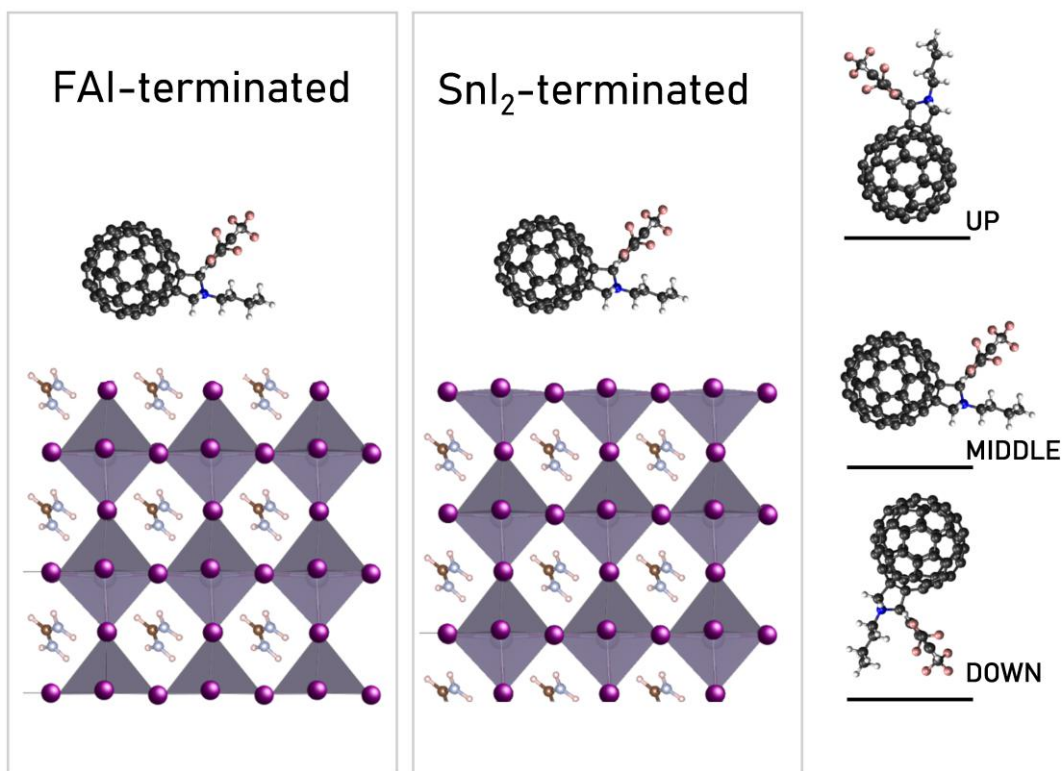
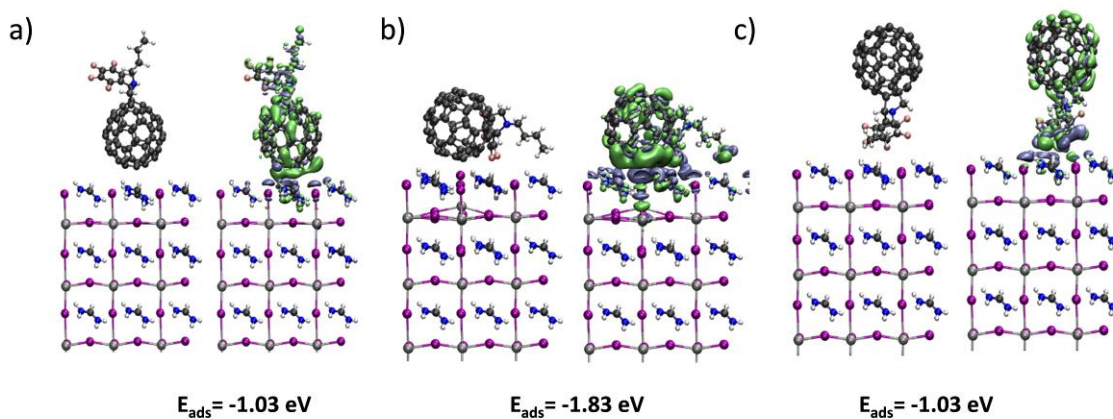


Figure S12. Fullerene derivative/FASnI₃ unit cells and relative orientations of the fullerene.

Table S3. Adsorption energies (eV) for different fullerene derivatives with different molecular orientations adsorbed on different perovskite surfaces.

Perovskite surface	FAI-terminated			SnI ₂ -terminated		
	Up	Middle	Down	Up	Middle	Down
C₆₀		-1.414			-0.876	
JM10	-1.032	-1.831	-1.028	-0.905	-1.579	-0.871
JM12	-1.092	-1.926	-1.052	-0.926	-1.909	-0.945

FAI-terminated



SnI₂-terminated

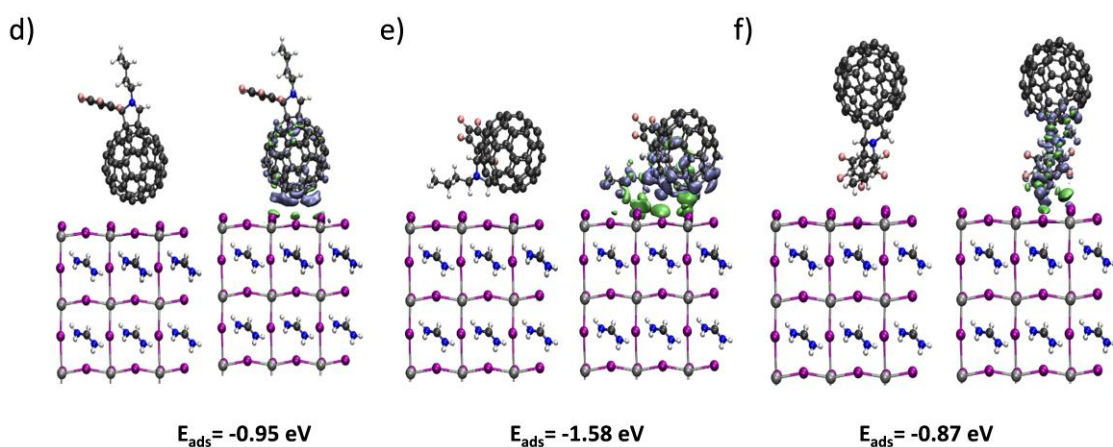
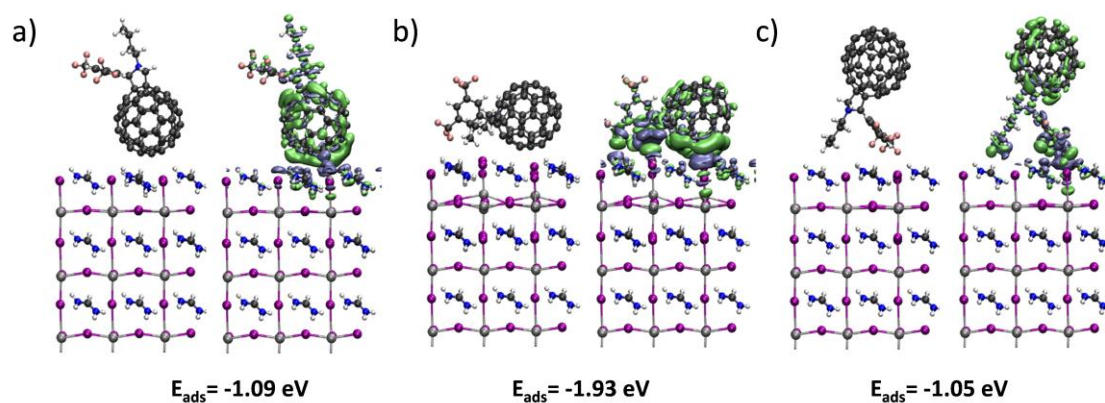


Figure S13. Isosurface of $\Delta\rho = 0.002$ a.u. for FASnI₃/JM10 systems: FAI-terminated surface interacting with a) fullerene cage (up), b) both fullerene and fluorinated moiety (middle), c) fluorinated moiety (down); SnI₂-terminated surface interacting with d) fullerene cage (up), e) both fullerene and fluorinated moiety (middle), f) fluorinated moiety (down). Green (Blue) regions represent positive (negative) values of $\Delta\rho$. Color code: carbon in black, hydrogen in white, nitrogen in blue, fluorine in pink, tin in grey and iodine in purple.

FAl-terminated



SnI₂-terminated

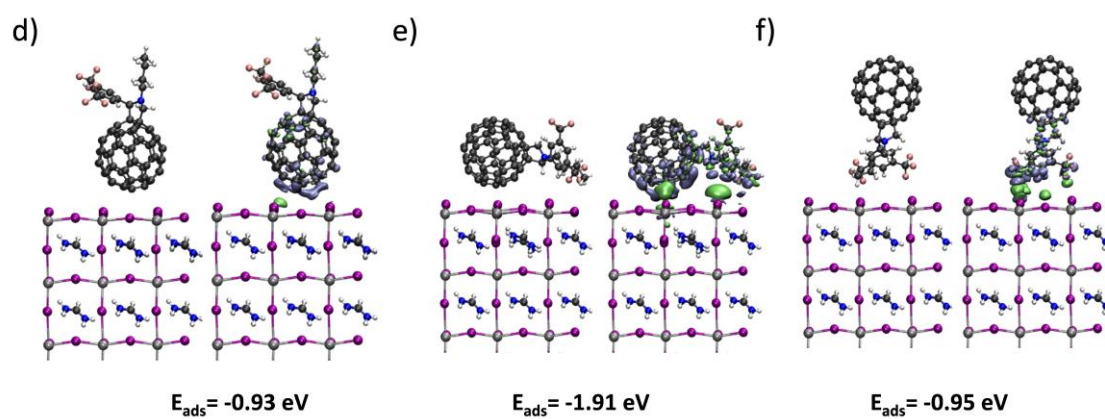


Figure S14. Isosurface of $\Delta\rho = 0.002 \text{ a.u.}$ for FASnI₃/JM12 systems: FAl-terminated surface interacting with a) fullerene cage (up), b) both fullerene and fluorinated moiety (middle), c) fluorinated moiety (down); SnI₂-terminated surface interacting with d) fullerene cage (up), e) both fullerene and fluorinated moiety (middle), f) fluorinated moiety (down). Green (Blue) regions represent positive (negative) values of $\Delta\rho$. Color code: carbon in black, hydrogen in white, nitrogen in blue, fluorine in pink, tin in grey and iodine in purple.

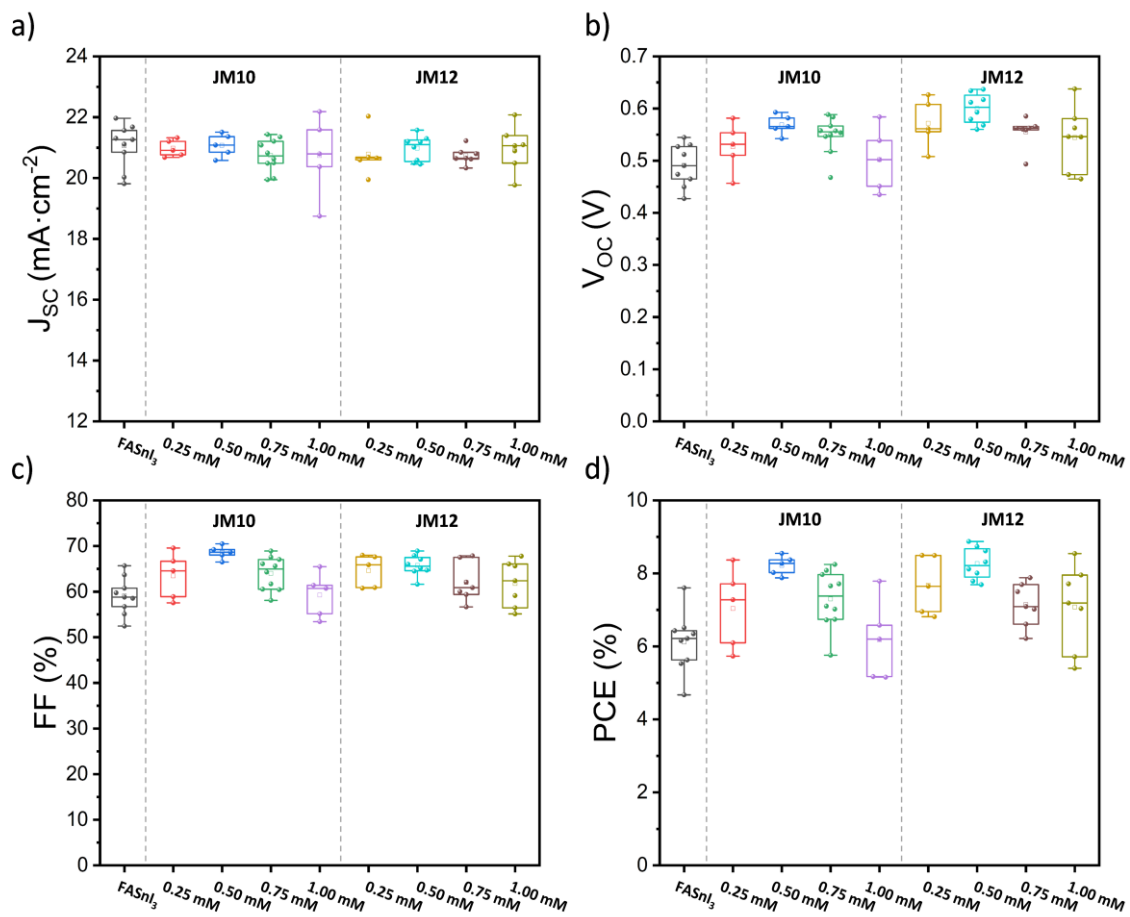


Figure S15. Statistics of the solar cell parameters with different concentrations of **JM10** and **JM12**: (a) J_{SC} , (b) V_{OC} , (c) FF and (d) PCE. All the parameters were extracted from J - V curves under $100 \text{ mW}\cdot\text{cm}^{-2}$ AM 1.5 G illumination.

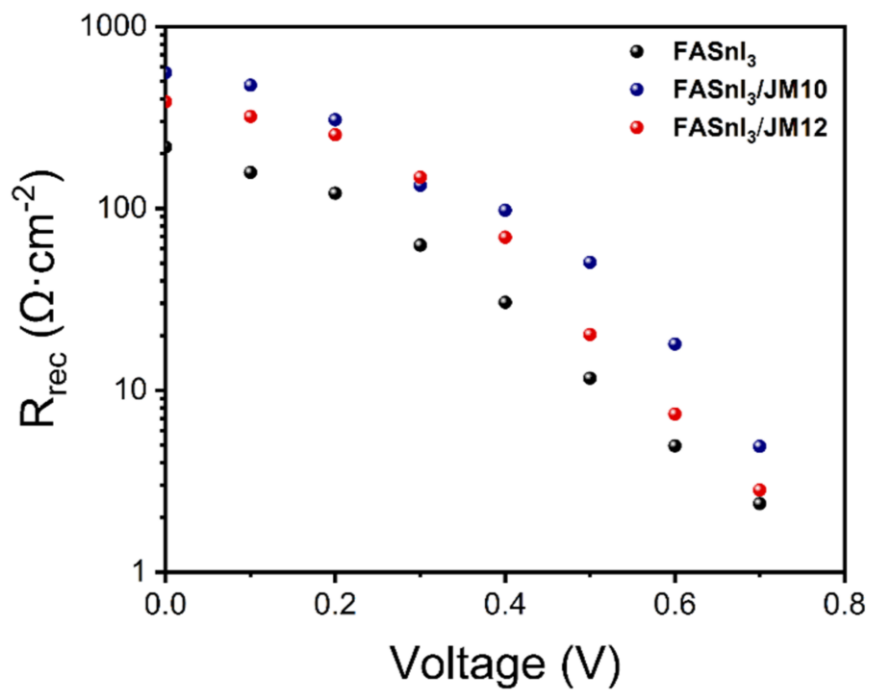


Figure S16. Recombination resistance (R_{rec}) from impedance spectroscopy under 1 sun illumination for samples with and without **JM10** and **JM12**.

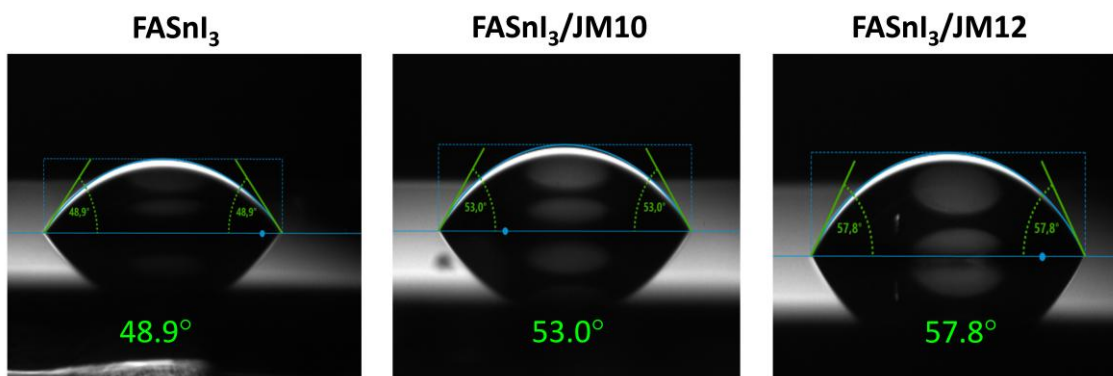


Figure S17. Contact angle of water droplets on the different surfaces.

References

1. Sanchez-Diaz, J.; Sánchez, R. S.; Masi, S.; Krečmarová, M.; Alvarez, A. O.; Barea, E. M.; Rodriguez-Romero, J.; Chirvony, V. S.; Sánchez-Royo, J. F.; Martinez-Pastor, J. P.; Mora-Seró, I., Tin perovskite solar cells with >1,300 h of operational stability in N₂ through a synergistic chemical engineering approach. *Joule* **2022**, *6* (4), 861-883.
2. Zou, Y.; Najari, A.; Berrouard, P.; Beaupré, S.; Réda Aïch, B.; Tao, Y.; Leclerc, M., A Thieno[3,4-c]pyrrole-4,6-dione-Based Copolymer for Efficient Solar Cells. *Journal of the American Chemical Society* **2010**, *132* (15), 5330-5331.
3. Cardona, C. M.; Li, W.; Kaifer, A. E.; Stockdale, D.; Bazan, G. C., Electrochemical Considerations for Determining Absolute Frontier Orbital Energy Levels of Conjugated Polymers for Solar Cell Applications. *Advanced Materials* **2011**, *23* (20), 2367-2371.
4. Kresse, G.; Hafner, J., Ab initio molecular dynamics for liquid metals. *Physical Review B* **1993**, *47* (1), 558-561.
5. Kresse, G.; Hafner, J., Ab initio molecular-dynamics simulation of the liquid-metal--amorphous-semiconductor transition in germanium. *Physical Review B* **1994**, *49* (20), 14251-14269.
6. Kresse, G.; Hafner, J., Norm-conserving and ultrasoft pseudopotentials for first-row and transition elements. *Journal of Physics: Condensed Matter* **1994**, *6* (40), 8245.
7. Kresse, G.; Furthmüller, J., Efficiency of ab-initio total energy calculations for metals and semiconductors using a plane-wave basis set. *Computational Materials Science* **1996**, *6* (1), 15-50.
8. Kresse, G.; Furthmüller, J., Efficient iterative schemes for ab initio total-energy calculations using a plane-wave basis set. *Physical Review B* **1996**, *54* (16), 11169-11186.
9. Kresse, G.; Joubert, D., From ultrasoft pseudopotentials to the projector augmented-wave method. *Physical Review B* **1999**, *59* (3), 1758-1775.
10. Neese, F.; Wennmohs, F.; Becker, U.; Riplinger, C., The ORCA quantum chemistry program package. *The Journal of Chemical Physics* **2020**, *152* (22).
11. Klimeš, J.; Bowler, D. R.; Michaelides, A., Chemical accuracy for the van der Waals density functional. *Journal of Physics: Condensed Matter* **2010**, *22* (2), 022201.
12. Dion, M.; Rydberg, H.; Schröder, E.; Langreth, D. C.; Lundqvist, B. I., Van der Waals Density Functional for General Geometries. *Physical Review Letters* **2004**, *92* (24), 246401.
13. Román-Pérez, G.; Soler, J. M., Efficient Implementation of a van der Waals Density Functional: Application to Double-Wall Carbon Nanotubes. *Physical Review Letters* **2009**, *103* (9), 096102.
14. Klimeš, J.; Bowler, D. R.; Michaelides, A., Van der Waals density functionals applied to solids. *Physical Review B* **2011**, *83* (19), 195131.
15. Schäfer, A.; Huber, C.; Ahlrichs, R., Fully optimized contracted Gaussian basis sets of triple zeta valence quality for atoms Li to Kr. *The Journal of Chemical Physics* **1994**, *100* (8), 5829-5835.
16. Weigend, F., Accurate Coulomb-fitting basis sets for H to Rn. *Physical Chemistry Chemical Physics* **2006**, *8* (9), 1057-1065.
17. Weigend, F.; Ahlrichs, R., Balanced basis sets of split valence, triple zeta valence and quadruple zeta valence quality for H to Rn: Design and assessment of accuracy. *Physical Chemistry Chemical Physics* **2005**, *7* (18), 3297-3305.
18. Grimme, S.; Antony, J.; Ehrlich, S.; Krieg, H., A consistent and accurate ab initio parametrization of density functional dispersion correction (DFT-D) for the 94 elements H-Pu. *The Journal of Chemical Physics* **2010**, *132* (15).

19. Zhang, J.; Lu, T., Efficient evaluation of electrostatic potential with computerized optimized code. *Physical Chemistry Chemical Physics* **2021**, *23* (36), 20323-20328.
20. Lu, T.; Chen, F., Multiwfn: A multifunctional wavefunction analyzer. **2012**, *33* (5), 580-592.
21. Kahmann, S.; Nazarenko, O.; Shao, S.; Hordiichuk, O.; Kepenekian, M.; Even, J.; Kovalenko, M. V.; Blake, G. R.; Loi, M. A., Negative Thermal Quenching in FASnI₃ Perovskite Single Crystals and Thin Films. *ACS Energy Letters* **2020**, *5* (8), 2512-2519.
22. Peng, L.; Xie, W., Theoretical and experimental investigations on the bulk photovoltaic effect in lead-free perovskites MASnI₃ and FASnI₃. *RSC Advances* **2020**, *10* (25), 14679-14688.
23. Erten-Ela, S.; Villegas, C.; Delgado, J. L.; Martín, N., Pyrrolidino [60] and [70]fullerene homo- and heterodimers as electron acceptors for OPV. *New Journal of Chemistry* **2015**, *39* (2), 1477-1482.